Applied Surface Science 535 (2021) 147480

Contents lists available at ScienceDirect

Applied Surface Science

journal homepage: www.elsevier.com/locate/apsusc

Staggered band offset induced high performance opto-electronic devices: Atomically thin vertically stacked GaSe-SnS_2 van der Waals p-n heterostructures

Packiyaraj Perumal[a,b], Rajesh Kumar Ulaganathan[c], Raman Sankar[c], Ling Zhu[a,*]

[a] College of Physics and Optoelectronic Engineering, Shenzhen University, Shenzhen 518060, PR China
[b] Department of Physics, National Taiwan University, No. 1, Sec. 4, Roosevelt Road, Taipei 106, Taiwan
[c] Center for Condensed Matter Sciences, National Taiwan University, No. 1, Sec. 4, Roosevelt Road, Taipei 106, Taiwan

ARTICLE INFO

Keywords:
van der Waals 2D heterojunctions
GaSe-SnS_2
Photodiodes
Photovoltaic
Type II band structure

ABSTRACT

Atomically thin vertically stacked 2D vdW heterostructures have recently emerged as a new kind of device with intriguing novel phenomena for both academic and industrial interests. However, the lack of p-type materials remains a challenging issue to create useful devices for the realization of practical applications. Here, we demonstrate the first vertically stacked few-layered *p*-type GaSe and *n*-type SnS_2 vdW heterostructure for high-performance optoelectronic applications. It is found that the phototransistors based on a few-layered GaSe/SnS_2 p-n junction show superior performance with the responsivity, EQE and specific detectivity as high as ~35 AW^{-1}, 62%, and 8.2 × 10^{13} J, respectively, which exceed all the reported values derived from 2D materials. Also, the GaSe/SnS_2 p-n junction can serve as a photovoltaic cell with a high power conversion efficiency of about ~2.84%. Moreover, the heterostructures can be deposited on flexible PET substrates with excellent performance. Through a detailed study, the underlying mechanism responsible for the high performance can be attributed to the unique type II band alignment and excellent quality of the interface. The heterojunctions presented in this work demonstrate a new illustration for the stacking of 2D materials, which is very useful for the development of next-generation novel optoelectronic devices.

1. Introduction

Recently, several two-dimensional (2D) crystals with superior performance have been discovered and sparked broad interest on the stacking of 2D materials through van der Waals (vdW) heterostructures, making them feasible to create a wide range of heterojunctions in a new frontier of modern semiconductor industry [1–4]. In this regard, unlike conventional heterostructures, 2D heterostructures are emerging as an ideal platform for their potential applications in atomically thin electronics, optoelectronics, and light-harvesting [5–9]. Relatively, various distinct frameworks of heterojunctions, created by lateral and vertical stacking of several 2D crystals have stimulated intensive research for new kinds of 2D heterostructures [10–11]. Usually, heterojunctions applied in the optoelectronic devices require anisotype, i.e., *p-n* heterojunctions, which consist of two semiconductors with dissimilar types of charge carriers. However, even though vertically stacked p-n heterostructures based on 2D materials have been studied in several published works due to their great potential applications, the reported performance remains a large room for improvement [12–15]. Especially, carrier transport in the vertical heterostructures based on p and n-type materials with sharp and clean interfaces has become promising and remains challenging, which is desirable for the realization of unprecedented functional device applications by the interlayer coupling [16–20]. These heterostructures have fascinated considerable scrutiny and opened up a new pavement for exploring novel optoelectornic device applications, such as high-mobility field-effect transistors (FETs), tunable p-n junction photo-diodes, LEDs, solar cells and sensors.

Until now, various 2D vdW heterostructures, including WSe_2/MoS_2, WS_2/MoS_2, p/n-MoS_2 and MoS_2/black phosphorus, have been reported recently for novel optoelectronics applications [21–22]. Among them, the new 2D materials-based optoelectronic devices, particularly of an anisotype heterojunction, possess a wide combination of various 2D materials and exhibit novel functional properties with remarkable strong light-matter interactions for future prospectives [23–24]. For example, a switchable bidirectional charge transport has been developed, instead of the unidirectional charge transport in a traditional *p–n*

* Corresponding author.
E-mail address: zhuling@szu.edu.cn (L. Zhu).

https://doi.org/10.1016/j.apsusc.2020.147480
Received 9 April 2020; Received in revised form 29 June 2020; Accepted 6 August 2020
Available online 09 August 2020
0169-4332/

heterojunction [25]. Recently, the generations of photocurrent and electroluminescence from a vertical p-n junction between p-WSe_2/n-MoS_2 have been reported [26]. Also, the electrostatic-gating-induced lateral p-n junction between WSe_2/black phosphorus has been realized for photodetectors, solar cells, and light-emitting diodes (LEDs) [27]. Notably, the tuning of Fermi levels at the vertical junction depends on the Thomas-Fermi screening of the bottom constituent nanoflakes of a vertical heterojunction, which only works well for few-layered heterojunction [28–30]. Among the recent advances, gallium selenide (GaSe), an III-VI 2D layered semiconductor, has the planar tetra-layer (TL) structure in the unit cell, and consists of four covalent bonds in a series of Se-Ga-Ga-Se, a bandgap energy (E_g) of ~2.1 eV and an intrinsic *p*-type nature [31–32]. The advantage of GaSe is that it has a direct bandgap in the form of bulk and few-layered thickness (< 7 layers) compared to other TMDs [33]. Tin disulphide (SnS_2) is an *n*-type CdI_2-type crystal structure with a bandgap E_g ~ 2.3 eV, which has attracted great attention, for its abundance on earth and green optoelectronics. SnS_2 remains an indirect bandgap even when scaling down to monolayer from bulk counterpart [34]. Its intrinsic bandgap in the range of 1 to 3 eV is significant for optoelectronics, i.e., photodetectors, photovoltaic and flexible devices [35]. Considering all of these distinct features, it is foreseeable that p-GaSe/n-SnS_2 2D vdW heterostructure will possess many intriguing properties and make a promising building block for the development of optoelectronic devices with the functionalities of great significance.

In this paper, we introduced this new 2D vdW vertically stacked *p*-GaSe/*n*-SnS_2 heterojunctions formed by high-quality single crystals. In addition to the electrical characteristics, photodetector and photovoltaic behaviours of the junction were investigated. It is found that, the GaSe/SnS_2 p-n junction exhibits a high photoresponsivity (~35 A/W at λ = 633 nm, V_g = 30 V), external quantum efficiency (~62%) and specific detectivity (~8.2×10^{13} J). These excellent performances are much better than those of recently published 2D vdW p-n heterojunctions configured with other few-layered materials. Impressively, the GaSe/SnS_2 p-n heterojunction can serve as a photovoltaic cell with a high power conversion efficiency of about ~2.84%. Moreover, taking a step further, the optoelectronic characteristics of these heterojunction devices on a flexible PET substrate were scrutinized with and without bending, showing good endurance and retention. These observations indicate that atomically thin vertically stacked 2D p-GaSe/n-SnS_2 vdW heterostructures can be featured as an excellent candidate for the feasibility of various functionalities.

2. Results

Fig. 1**a** shows the schematic illustration of the atomic configuration of vertically stacked *p*-GaSe/n-SnS_2 vdW heterostructure. The schematics of the individual layer of GaSe and SnS_2 are shown in Figure S1 in the Supporting Information. Fig. 1b presents an optical microscope (OM) image of a GaSe/SnS_2 vertical heterojunction device with a clear enhanced colour contrast between the layer interface. The devices were fabricated by micromechanical cleavage technique and explained in the experimental section. Fig. 1c reveals the single-crystal X-ray diffraction (XRD) of GaSe and SnS_2 crystals grown by chemical vapor transport (CVT) method, which is identical to the previously reported diffraction patterns [36–37]. Fig. 1d shows the Raman spectra of an GaSe/SnS_2 heterostructure, which includes the Raman modes from the constituent layers (Figure S2 in the Supporting Information). The peak positions at ~208 nm (E_g) and ~316 (A^2_{1g}) can be assigned to the Raman active modes for 2D SnS_2 [38,39], and the Raman spectra of a GaSe crystals exhibit 4 peaks at ~137 nm (A^1_{1g}), 216 nm (E^1_{2g}), ~ 250 nm (E^2_{1g}), and ~305 nm (A^2_{1g}), which are also consistent with previous reports [40–41].

Fig. 2**a** shows an OM image of a vertical p-n heterojunction diode with the deposition of metallic electrodes for the electric and optoelectronic measurements. Briefly, a thin SnS_2 flake (~10.5 nm) were transferred on a Si/SiO_2 substrate, followed by transferring a GaSe flake (~25.5 nm) on top of the SnS_2 flake as shown in Fig. 2a. Throughout this work, a pair of Cr/Au (5/100 nm) electrodes were used as the source and drain electrodes in all of the devices, which were fabricated with a shadow mask using the thermal evaporation technique. Before the measurement of GaSe/SnS_2 heterojunction FETs, we have first analysed separately the electrical characteristic of few-layered SnS_2 and GaSe FETs to confirm the conductive nature of the channel materials. Figures S3 a and b show the V_g-dependent characteristics of SnS_2 and GaSe while sweeping the V_g from −60 V to + 60 V, respectively. The plots show that the current increases with increasing positive gate voltage for SnS_2-FET, indicating an n-type semiconductor behaviour. On the contrary, the current increases with decreasing negative gate voltage in GaSe-FET, consistent with the p-type characteristics. The Hall-effect measurement of the bulk SnS_2 and GaSe crystal evidence its *n*- and p-type nature, respectively, as shown in Figure S4. Figure S5 illustrates the schematic representation of the GaSe/SnS_2 p-n heterojunction device layout with the back gate electrode. Meanwhile, the I_{sd}-V_{sd} characteristics of the fabricated GaSe/SnS_2 FETs exhibit a clear current rectification behaviour as shown in Fig. 2b. The saturated current of the heterojunction was observed in reverse bias following the Shockley diode equation of $I = I_s$ (exp (V_{ds}/nV_t) −1), where I_s is the saturation current in the reverse bias regime, *n* is the ideality factor of the fabricated device, and V_t and V_{ds} are the thermal and bias voltages, respectively. Next, we probed the V_g-dependent output characteristics of the heterojunction by sweeping V_g from 0 to −70 V as shown in Fig. 2c. Interestingly, the applied negative V_g enhances the current in forward bias and maintains the saturated current in reverse bias. The fabricated heterojunction has a rectification ratio of ~10^2 at V_g = -30 V (Fig. 2d). These strong current-rectifying characteristics indicate that an excellent vdW p-n heterojunction spans between p-GaSe and n-SnS_2 layers.

As excellent rectification features were realized, the optoelectronic characteristics of our fabricated *p*-GaSe/*n*-SnS_2 heterojunction as a photodetector were examined. We measured the photoresponse of the *p*-GaSe/*n*-SnS_2 heterojunction, by using a 633 nm laser with different intensities of 0 (in the dark), 0.328, 1.6, 3.1 and 32.6 mW/cm^2 to illuminate the device as shown in Fig. 3**a**. The photocurrent (I_{photo}) was calculated by subtracting the dark current (I_{dark}) from the light-induced current (I_{light}), i.e., $I_{photo} = I_{light} - I_{dark}$. As seen in Fig. 3a, the I_{photo} in reverse bias is gradually enhanced with increasing illumination intensity, which shows that I_{photo} has a strong dependence on the incident power. The probable reason for the enhancement of the reverse current under illumination is due to the obvious photovoltaic effect. Next, we evaluated the performance of photodiode by calculating photoresponsivity (*R*) and external quantum efficiency (EQE) as follows. Fig. 3b exhibits the laser intensity-dependent *R,* defined as the ratio of the generated photocurrent to the total incident photon energy, i.e., $R = I_{ph}/(P_\lambda S)$ where P_λ and S are the incident light power and the illuminated area, respectively. The photoresponsivity of the p-n junction could reach R ~ 24.8 AW^{-1} at 633 nm of 0.326 mW/cm^2 illumination, which is the highest photoresponsivity achieved compared with other reported 2D p-n junctions. Additionally, note that R can be climbed to about ~35 AW^{-1} by simply changing the gate voltage (V_g = 30 V) as shown in Figure S6 in the Supporting Information.

The EQE (%) is defined as $hcR/e\lambda$, where *h* is Planck's constant, *c* is the velocity of the light, *R* is photoresponsivity of the device, *e* is the electron charge, and λ is the laser wavelength. Fig. 3c represents the EQE of the *p*-GaSe/*n*-SnS_2 junction, which could reach ~62% measured at 633 nm, V_{ds} = 10 V, and V_g = 0 V. Another critical parameter to determine the photodetection performance of a fabricated p-n junction is specific detectivity (D*). The D*is quantified by $D^* = A^{1/2} / NEP = R_\lambda A^{1/2} / (2eI_{dark})^{1/2}$, where R_λ, A, e and I_{dark} are the photoresponsivity, illuminated area, elementary charge, and dark current, respectively. Fig. 3d shows the D* versus illuminated laser power. Based on the measured parameter, the obtained D* ~8.2×10^{13}J for

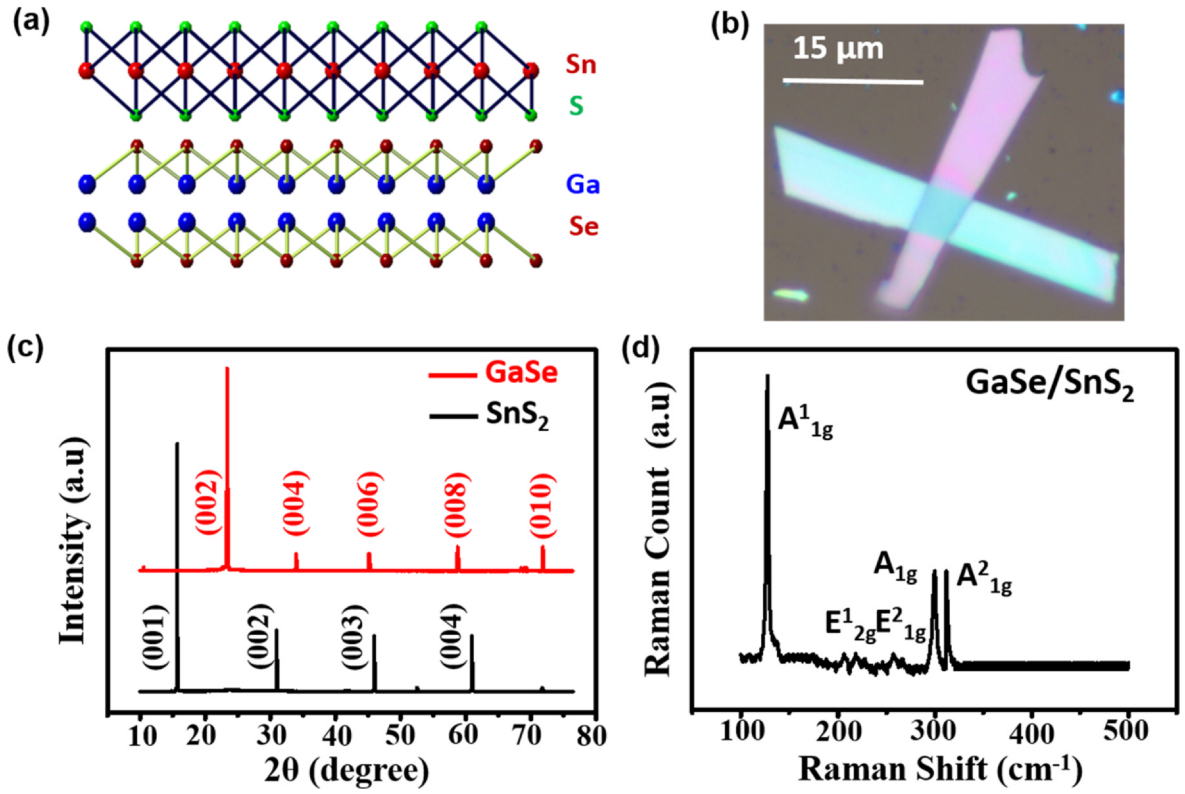

Fig. 1. (a) Schematic of the vertically stacked GaSe/SnS_2 heterostructure. (b) Optical microscope image of fabricated GaSe/SnS_2 heterostructure. (c) X-ray diffraction pattern of GaSe and SnS_2 single crystals. (d) Raman Spectra of GaSe/SnS_2 heterostructure.

the fabricated p-n heterojunction is higher than commercial silicon photodiodes (~10^{13} J) [42] and InGaAs (~10^{12} J to ~10^{13} J) [43].

Owing to the low dark current under reverse bias condition, excellent photoresponse performance was achieved. Furthermore, the time-resolved photoresponse was carried out to exhibit the response time (τ) of the GaSe/SnS_2 heterojunction photodiode. The I_{light} – t plot was measured with a continuation of on/off illumination using 633 nm laser. Fig. 3 (e-f) show the device response to one on/off illumination (P = 0.326 mWcm^{-2}), that exhibits a steep increase of photocurrent (I_{light}) underneath illumination and an instant drop after switched off. It is found that the rising time and falling time of the device are estimated to be ~9 ms and ~8 ms, respectively. Table 1 summarizes and compares the selected figures of merit between the GaSe/SnS_2 p-n junction and several other reported 2D layered p-n heterostructures. Based on the time-resolved measurement, The calculated frequency bandwidth of the device is ~12.8 Hz. If the response time (9 ms) is faster, the calculated bandwidth will be wider, because the response time can be also used to express as frequency response, which is the frequency when the photodetector output decreases by 3 dB. It is roughly approximated by $f_{3dB} \approx 0.35/t_r$, where t_r is the response time [49].

In addition to the electrical and photodetection characteristics of the junction discussed above, we explored the application of this junction as a photovoltaic cell. Fig. 4 represents the current density-voltage (J-V) characteristics device under AM 1.5G illumination. Under illumination, the open-circuit voltage (Voc) of 0.51 V, a short-circuit current density (Jsc) of 26.5 mA cm–2, and a fill factor (FF) of 0.42 were obtained, which leads to the power conversion efficiency (PCE) of 2.84% [19]. However, heterojunction formed between two different semiconductors having different energy bandgaps. The electric field formed due to the potential energy barrier between two dissimilar materials (p-GaSe/n-SnS2) at the interface is capable of separating the electrons and holes generated by absorption of light within the materials. Furthermore, being direct-bandgap at few-layer thickness, it allow high radiative efficiency. The strong absorption in atomically thin layers with sharp, clean interfaces allows the highest watt-per-gram utilization of the active material. Owing to their excellent electron-transport properties, high carrier mobility, direct bandgap and type II band alignment, shows its great potential to be used for low-cost, flexible, and highly efficient photovoltaic devices.

Moreover, to examine the further applicability, we deposit GaSe/SnS_2 2D vdW p-n heterojunctions on a high degree of flexible PET substrate, by the similar process as on silicon platforms as shown in Fig. 5**a**. Interestingly, the device of conducting p-n heterojunction channel can stick well onto the surface of the PET, revealing the potential capability of the device's flexibility. Subsequent thermal deposition of metal electrodes at both ends ensure mechanical flexibility. The power-dependent photocurrents recorded in each flat and bent states are shown in Fig. 5b and S7a in the Supporting Information, respectively, showing an equivalent performance compared with devices deposited on SiO_2/Si substrates.

The photocurrent increases with increasing laser power, yielding the highest photoresponsivity of ~3.8 AW^{-1} at a power density of 0.326 mWcm^{-2} as shown in Fig. 5c. To differentiate the p-GaSe/n-SnS_2 device performance on PET with flat and bending (a radius of ~2.5 cm), we observed that the responsivity within the bending state is reduced slightly compared with flat state, ie., the responsivity is slightly reduced to ~3.2 AW^{-1} under the same measured condition as shown in Fig. 5d and S7c in the Supporting Information. The responsivity was calculated under different bending radius as shown in Figure S8 in the Supporting Information, demonstrating bending durability. The reduced responsivity within the bending state is reasonable due to the possible mechanism that the erected tension in the bending state may additionally reduce the responsivity as a result of the variation of the band structure in the p-GaSe/n-SnS_2 channel and its relative optical properties [50–52]. These investigations reveal a promising potential of thin layered 2D vdW p-n heterojunctions for flexible and wearable optoelectronic applications.

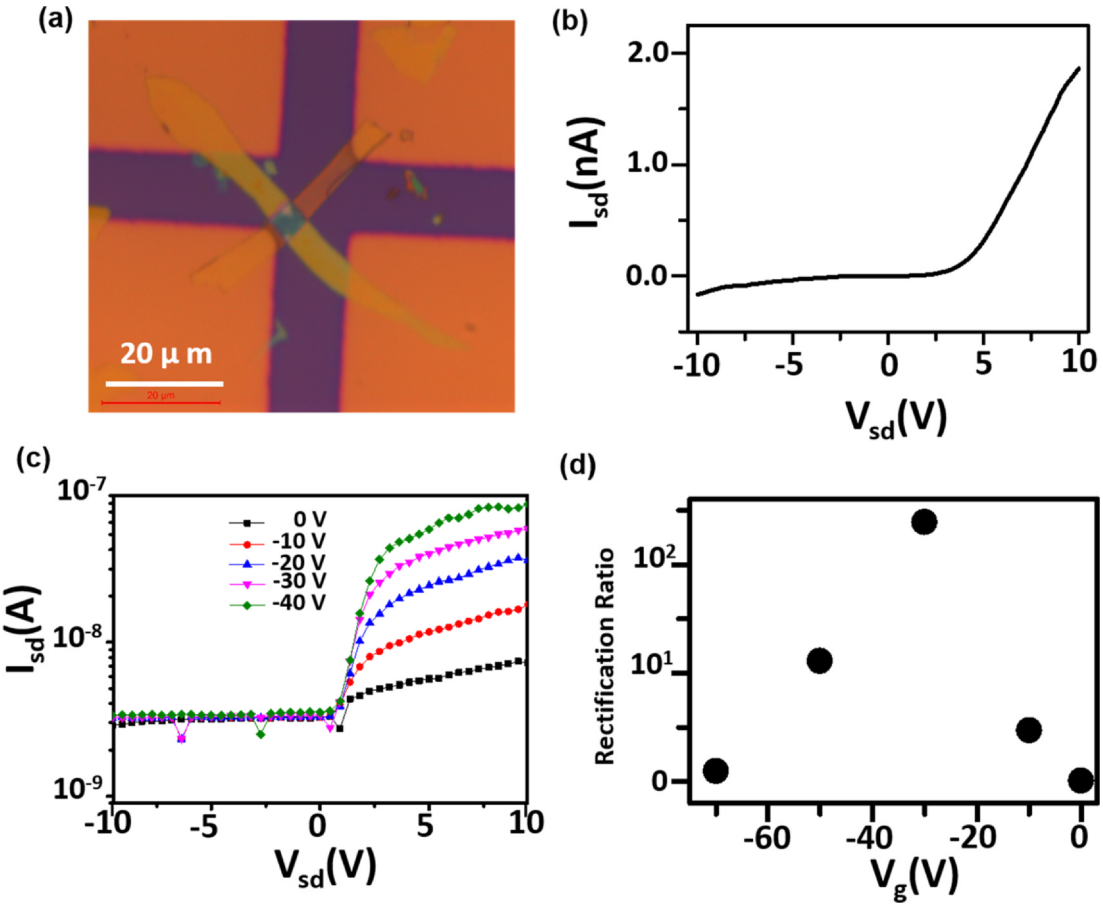

Fig. 2. (a) Optical microscope image of vertically stacked GaSe/SnS_2 heterostructure device. (b) I_{sd}-V_{sd} characteristics of p-n junction diode. (c) Gate tunable I-V characteristics. (d) Rectification ratio as a function of back-gate voltage (V_g).

3. Discussion

To find out the underlying mechanisms responsible for the high performance of GaSe/SnS_2 2D vdW p-n heterojunctions as observed above, we first look for the possibility of the unique band alignment. Fig. 6a and 6b show the schematic of the relative energy alignment of the conduction/valance bands of the constituent 2D materials before and after contact, respectively. The work functions (Φ) of GaSe and SnS_2 are 5.25 and 5.2 eV, respectively, adopted from literature reports [30,37,53–54]. The band alignment of the heterojunction belongs to type II as depicted in Fig. 6a and b. To obtain further evidence for supporting the type-II band alignment of GaSe/SnS_2 heterojunction, we have performed photoluminescence measurement. The PL spectra show two distinct peak positions, corresponding to two different layers. We have also performed PL spectra for each isolated GaSe and SnS_2 layers as shown in Figure S9 in the Supporting Information. Both of GaSe and SnS_2 layers show a strong PL intensity at their respective exciton position (2.11 eV and 2.28 eV, respectively), [29,40] which indicates the excellent crystallinity of the as-synthesized 2D single crystals. Quite interestingly, the PL intensity is significantly quenched for the heterostructure sample. Accordingly, the observation of the reduced PL intensity from GaSe/SnS_2 heterostructures reveals that an efficient charge transfer takes place in this heterojunction due to the type II band alignment. After photoexcitation, electrons transfer to the SnS_2 layer, while holes will like to stay in the GaSe layer.

Next, we explain the charge transport mechanism under varying the gate voltage in the junction region of *p*-GaSe/*n*-SnS_2 with the help of the band alignment as shown in Fig. 6. The advantage of ultrathin materials in vertical heterostructures allows the penetration of the electric field from the back gate through the entire stack, thereby enabling gate tunability of the heterointerface. This unique feature is not feasible in the heterojunction formed by bulky semiconductors due to Thomson-Fermi screening [26–28]. In this work, the fabricated p-n junction consists of the bottom few-layered flakes of SnS_2 (~10.5 nm) on a SiO_2/Si substrate and the top flakes of GaSe (~25.2 nm). The heterojunction formed by a few-layered GaSe/SnS_2/SiO_2/Si allows tuning the Fermi level of the bottom few-layered SnS_2 by the gate field and also affecting the top GaSe layer. In the equilibrium condition, no current passes through the GaSe/SnS_2 junction. Under forward bias condition, the height of the developed built-in potential of the junction is reduced, which allows the transfer of electrons from *n*-SnS_2 to *p*-GaSe over the lower barrier due to the gate field as shown in Figure S10 in the Supporting Information. Consequently, fewer electrons transport over the junction from *n*-SnS_2 to *p*-GaSe as evidenced experimentally shown in Figure S6 in the Supporting Information. On the other hand, under reverse bias, the built-in potential at the interface of the *p-n* junction is enhanced, which prohibits electrons moving from SnS_2 to GaSe. As a result, a significant reverse current is observed because electrons now can easily transfer from GaSe to SnS_2.

The high photoresponsivity (R) of the vdW GaSe/SnS_2 p-n junction can be attributed to the following reasons. (1) Because of the type II band alignment and the existence of a strong built-in potential in the p-n heterojunction, the photogenerated electron-hole pairs can be efficiently separated and it leads to the increased lifetime of photogenerated carriers. (2) The high carrier mobilities of SnS_2 (~4.6 V^{-1} cm^2 S^{-1}) [50] and GaSe (~0.6 V^{-1} cm^2 S^{-1}) [55] also play an important role. (3) Intrinsic characteristics of good quality of both p-GaSe and n-SnS_2 single crystals contain much less scattering from foreign atomic dopants. (4) The few-layered thickness of the bottom layer (~10.5 nm thin SnS_2) provides a better screening effect against the Coulomb

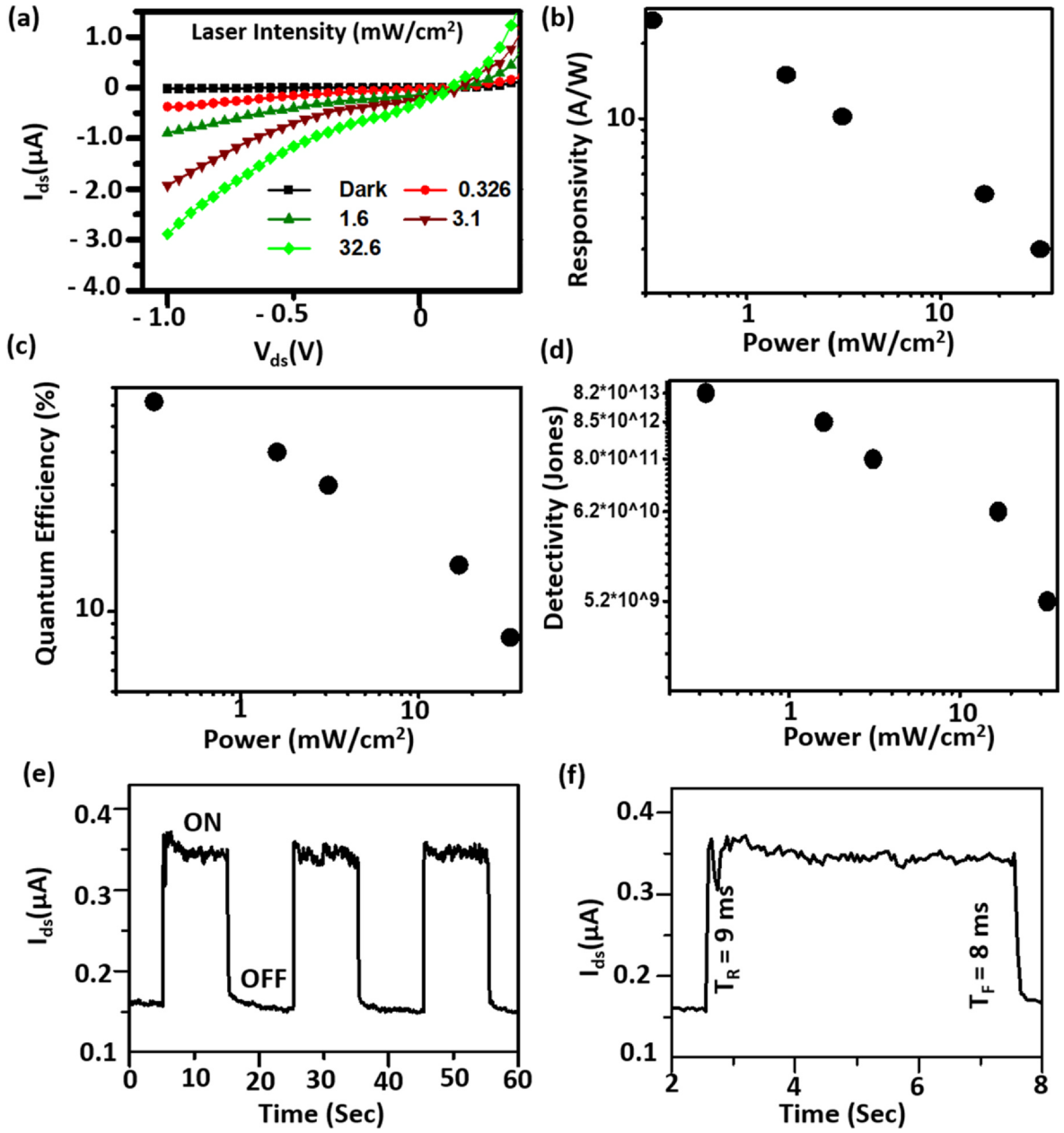

Fig. 3. Photoresponse study of vertically stacked p-GaSe/n-SnS_2 heterostructure device on SiO_2/Si substrate. (a) Photoconductivity spectra of vertically stacked GaSe/SnS_2 photodiode at dark and various illuminated power intensities (Dark, 0.326, 1.6, 3.1, and 32.6 mW/cm^2). (b) The plot of responsivity versus power intensity. (c) The plot of quantum efficiency versus power intensity. (d) The plot of detectivity versus power intensity. (e,f) The time-dependent photoresponse characteristics of the device.

Table 1
Summary of performance metrices of 2D vdW crystal based p-n heterostructure.

Materials	Responsivity (A/W)	Detectivity	Response time	Ref.
Monolayer MoS_2/WSe_2	0.011	—	—	[44]
Few-layered MoS_2/WSe_2	0.125	—	—	[20]
Few-layered MoS_2/WSe_2	1.42	—	—	[45]
Few-layered MoS_2/BP	3.54	—	—	[46]
Few-layered MoS_2/WSe_2	5.07	3.0×10^{10}	—	[47]
Few-layered GaTe/MoS_2	21.83	8.4×10^{13}	~7 ms	[48]
Few-layeredGaSe/SnS_2 on SiO_2/Si	24.8	8.2×10^{13}	~8 ms	Present work
	35.2 (V_g = 30 V)	——	——	Present Work
Few-layered GaSe/SnS_2 on PET	3.8 (planar state)	—	–	Presentwork
	3.2 (bent state)(bent state)	—	–	Presentwork

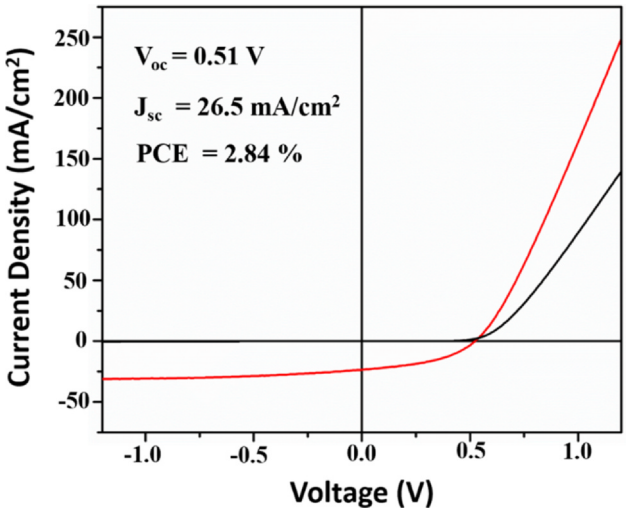

Fig. 4. *J-V* characteristics of p-GaSe/n-SnS_2 heterostructure measured with and without the illumination of AM 1.5 G solar simulator.

scattering [56].

4. Conclusion

In summary, we have successfully demonstrated the fabrication of vertically stacked few-layered vdW p-GaSe/n-SnS_2 heterostructures, which enables a gate tunable electronic and optoelectronic characteristics. The electrical characteristics of the junction exhibit excellent current rectification behaviour. We show that the rectifier behavior of the heterojunction provides a useful route to manipulate the performance of phototransistor. The GaSe/SnS_2 p-n junction can serve as an excellent photodetector with a responsivity of about ~35 A/W, an external quantum efficiency as high as 62%, and a selective detectivity of 8.2×10^{13} J, which is even higher than commercial Si/InGaAs photodetectors. Furthermore, we demonstrate the application of this junction as a photovoltaic cell and the measured power conversion efficiency is about ~2.84%. Moreover, we also demonstrate this new type of heterojunction on flexible PET substrates with excellent performance. All these findings demonstrate that GaSe/SnS_2 vdW p-n junctions have attractive potential applications in both electronic and optoelectronic devices. Therefore, our work shown here provides a new illustration for the vertically stacked 2D vdW heterostructures with various novel properties, which is very useful for the development of not-yet realized devices.

5. Experimental section

5.1. Material synthesis

A technique called chemical vapor transport (CVT) is used for synthesizing single-crystalline p-type GaSe and n-type SnS_2 semiconductors. Using iodine as the transport agent, GaSe single crystals were synthesized. In a quartz tube, 99.999% pure Ga powder and Se pellets were introduced with pure Iodine (5.8 mg of 1 per cm3). At a temperature gradient of ~100 ˚C, the quartz tube was vacuumed up to 1150 ˚C for 1.5 weeks and cooled to 1050 ˚C at a rate of 10 ˚C/h followed by another cool down to 800 ˚C at a rate of 2 ˚C/h for 2 days and subsequently quenched in air. In our previous reports, growth methods

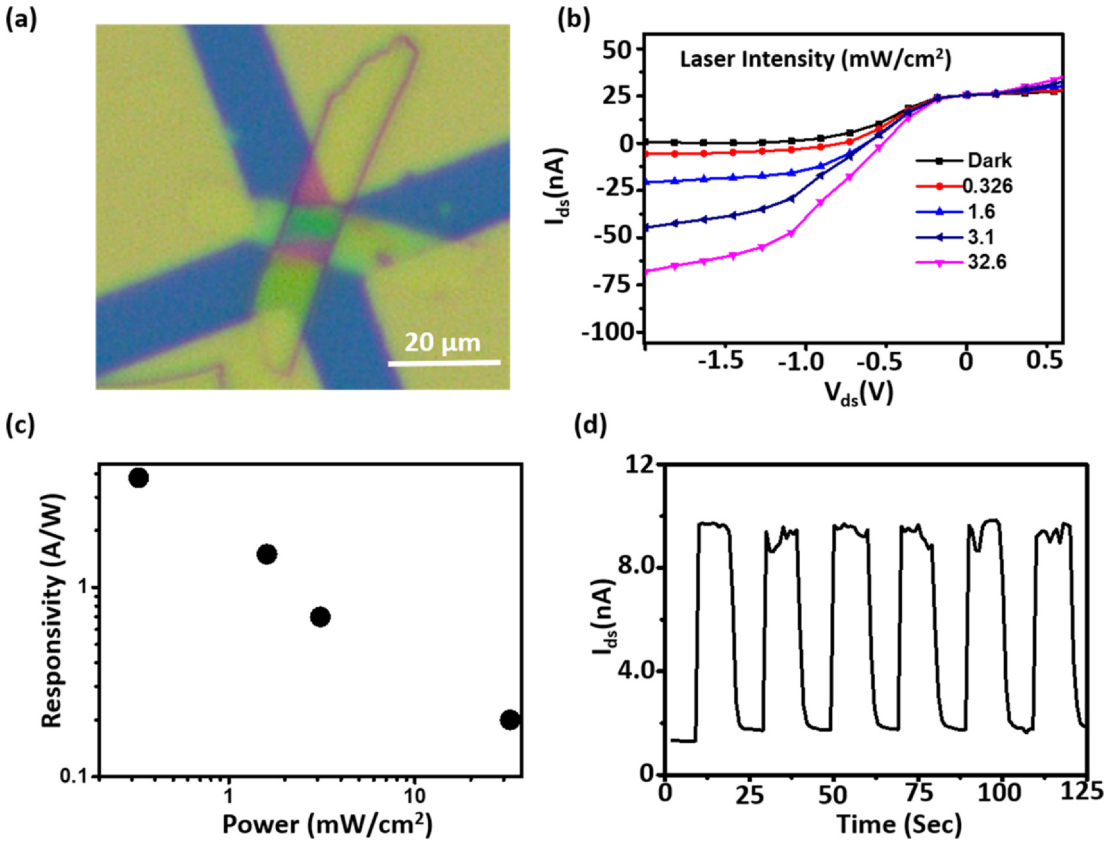

Fig. 5. Optoelectronic performance of van der Waals heterostructure deposited on flexible PET substrate. (a) Optical microscope image of vertically stacked GaSe/SnS_2 heterostructure on PET substrate. (b) Photoconductivity spectra of vertically stacked GaSe/SnS_2 photodiode on PET, performed at flat state with various illuminated power intensities (Dark, 0.326, 1.6, 3.1, and 32.6 mW/cm^2). (c) The plot of responsivity versus power intensity. (d) The photoswitching measurement of the device on a flexible PET substrate.

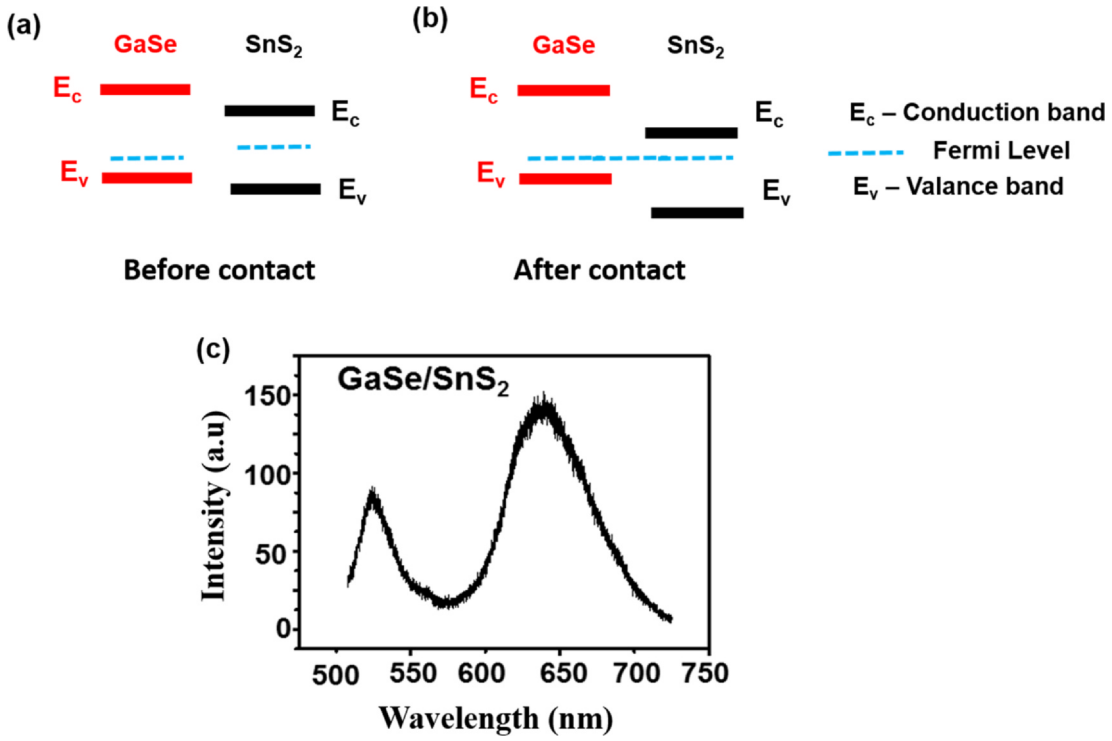

Fig. 6. Schematic of the band alignment of GaSe/SnS_2 heterostructure, which forms a type II heterojunction. (a) Before contact, (c) After contact and (c) Typical photoluminescence spectra of GaSe/SnS_2 heterostructure.

of SnS_2 were described [40].

5.2. Characterization

The X-ray diffractometry (SmartLab, Rigaku) with Cu Kα radiation (λ = 154059 Å) and Bragg–Brentano geometry were used for investigating the crystal structures of all the grown crystals. The mechanical exfoliation method is used for preparing flakes of GaSe and SnS_2 with few-layer thickness and transferred to SiO_2 (300 nm)/Si substrate. Optical microscopy (Olympus, BX 51 M) equipped with a charge-coupled device (CCD) camera (Leica, DFC495) was used to observe the morphology of the exfoliated flakes. The confocal Raman spectrometer (Jobin Yvon, LabRAM HR800) with a 30 s exposure time and a 532 nm wavelength laser is used for individual measurement of Raman spectra of GaSe and SnS_2 flakes and at junction area.

5.3. Device Fabrication and Characterization

All the heterostructures after aligning shadow mask were fabricated and Cr/Au (5/100 nm) were evaporated as the source and drain electrodes. A laser diode (633 nm wavelength) and an electrical characterization system (Keithley 2636 source meter, Keithley Instruments) were used in measuring the optical and electrical characteristics of the devices.

Declaration of Competing Interest

The authors declare that they have no known competing financial interests or personal relationships that could have appeared to influence the work reported in this paper.

Acknowledgements

This work was financially supported by the grants from Guangdong Basic and Applied Basic Research Foundation(Grant no: 2019A1515011762), Shenzhen Science and Technology Innovation Foundation (Grant no: JCYJ20180305125302333, JCYJ20170818093035338, JCYJ20180305125430954), Shenzhen University fund (Grant no: 860-000002110229) and Foshan City Education Department Fundation.

Received: ((will be filled in by the editorial staff))
Revised: ((will be filled in by the editorial staff))
Published online: ((will be filled in by the editorial staff))

Appendix A. Supplementary material

Supplementary data to this article can be found online at https://doi.org/10.1016/j.apsusc.2020.147480.

References

[1] A.K. Geim, I.V. Grigorieva, Nature 499 (2013) 419.
[2] D. Jariwala, T.J. Marks, M.C. Hersam, Nat. Mater. 16 (2017) 170.
[3] V.W. Brar, A.R. Koltonow, J. Huang, ACS Photon. 4 (2017) 407.
[4] J.Y. Lee, J.H. Shin, G.H. Lee, C.H. Lee, Nanomaterials (Basel) 6 (2016) 11.
[5] W.J. Yu, Q.A. Vu, H. Oh, H.G. Nam, H. Zhou, S. Cha, J.Y. Kim, A. Carvalho, M. Jeong, H. Choi, A.H. Castro Neto, Y.H. Lee, X. Duan, Nat. Commun. 7 (2016) 13278.
[6] K.S. Novoselov, A. Mishchenko, A. Carvalho, A.H. Castro Neto, Science 353 (2016) aac9439.
[7] F. Bonaccorso, L. Colombo, G. Yu, M. Stoller, V. Tozzini, A.C. Ferrari, R.S. Ruoff, V. Pellegrini, Science 347 (2015) 1246501.
[8] Q.A. Vu, J.H. Lee, V.L. Nguyen, Y.S. Shin, S.C. Lim, K. Lee, J. Heo, S. Park, K. Kim, Y.H. Lee, W.J. Yu, Nano Lett. 17 (2017) 453.
[9] Q.A. Vu, Y.S. Shin, Y.R. Kim, V.L. Nguyen, W.T. Kang, H. Kim, D.H. Luong, I.M. Lee, K. Lee, D.S. Ko, J. Heo, S. Park, Y.H. Lee, W.J. Yu, Nat. Commun. 7 (2016) 12725.
[10] Y. Gong, J. Lin, X. Wang, G. Shi, S. Lei, Z. Lin, X. Zou, G. Ye, R. Vajtai, B.I. Yakobson, H. Terrones, M. Terrones, B.K. Tay, J. Lou, S.T. Pantelides, Z. Liu, W. Zhou, P.M. Ajayan, Nat. Mater. 13 (2014) 1135.
[11] X. Ling, Y. Lin, Q. Ma, Z. Wang, Y. Song, L. Yu, S. Huang, W. Fang, X. Zhang, A.L. Hsu, Y. Bie, Y.H. Lee, Y. Zhu, L. Wu, J. Li, P. Jarillo-Herrero, M. Dresselhaus, T. Palacios, J. Kong, Adv. Mater. 28 (2016) 2322.
[12] X. Duan, C. Wang, J.C. Shaw, R. Cheng, Y. Chen, H. Li, X. Wu, Y. Tang, Q. Zhang, A. Pan, J. Jiang, R. Yu, Y. Huang, X. Duan, Nat. Nanotechnol. 9 (2014) 1024.
[13] Y. Wang, W.X. Zhou, L. Huang, C. Xia, L.M. Tang, H.X. Deng, Y. Li, K.Q. Chen, J. Li, Z. Wei, 2D Mater. 4 (2017) 025097.
[14] Y. Deng, Z. Luo, N.J. Conrad, H. Liu, Y. Gong, S. Najmaei, P.M. Ajayan, J. Lou,

X. Xu, P.D. Ye, ACS Nano 8 (2014) 8292–8299.
[15] M.H. Doan, Y. Jin, S. Adhikari, S. Lee, J. Zhoa, S.C. Lim, Y.H. Lee, ACS Nano 11 (2017) 3832–3840.
[16] T. Roy, M. Tosun, X. Cao, H. Fang, D.H. Lien, P. Zhao, Y.Z. Chen, Y.L. Chueh, J. Guo, A. Javey, ACS Nano 9 (2015) 2071–2079.
[17] H. Tan, Y. Fan, Y. Zhou, Q. Chen, W. Xu, J.H. Warner, ACS Nano 10 (2016) 7866–7873.
[18] A. Pezeshki, S.H.H. Shokouh, T. Nazari, K. Oh, S. Im, Adv. Mater. 28 (2016) 3216–3222.
[19] M.L. Tsai, M.Y. Li, J.R.D. Retamal, K.T. Lam, Y.C. Lin, K. Suenaga, L.J. Chen, G. Liang, L.J. Li, J.H. He, Adv. Mater. (2017) 1701168.
[20] C.H. Lee, G.H. Lee, A.M. van der Zande, W.C. Chen, Y.L. Li, M.Y. Han, X. Cui, G. Arefe, C. Nuckolls, T.F. Heinz, J. Guo, J. Hone, P. Kim, Nat. Nanotechnol. 9 (2014) 676–681.
[21] H.M. Hill, A.F. Rigosi, K.T. Rim, G.W. Flynn, T.F. Heinz, Nano Lett. 16 (2016) 4831.
[22] X. Hong, J. Kim, S.F. Shi, Y. Zhang, C. Jin, Y. Sun, S. Tongay, J. Wu, Y. Zhang, F. Wang, Nat. Nanotechnol. 9 (2014) 682.
[23] X. Liu, T. Galfsky, Z. Sun, F. Xia, E.-C. Lin, Y.-H. Lee, S. Kéna-Cohen, V.M. Menon, Nat. Photonics 9 (2014) 30.
[24] W. Aggoune, C. Cocchi, D. Nabok, K. Rezouali, M. Akli Belkhir, C. Draxl, J. Phys. Chem. Lett. 8 (2017) 1464.
[25] M. Buscema, D.J. Groenendijk, G.A. Steele, H.S. van der Zant, A. Castellanos-Gomez, Nat. Commun. 5 (2014) 4651.
[26] R. Cheng, D. Li, H. Zhou, C. Wang, A. Yin, S. Jiang, Y. Liu, Y. Chen, Y. Huang, X. Duan, Nano Lett. 14 (2014) 5590.
[27] J.S. Ross, P. Klement, A.M. Jones, N.J. Ghimire, J. Yan, D.G. Mandrus, T. Taniguchi, K. Watanabe, K. Kitamura, W. Yao, D.H. Cobden, X. Xu, Nat. Nanotechnol. 9 (2014) 268.
[28] T. Georgiou, R. Jalil, B.D. Belle, L. Britnell, R.V. Gorbachev, S.V. Morozov, Y.J. Kim, A. Gholinia, S.J. Haigh, O. Makarovsky, L. Eaves, L.A. Ponomarenko, A.K. Geim, K.S. Novoselov, A. Mishchenko, Nat. Nanotechnol. 8 (2013) 100–103.
[29] H. Yang, J. Heo, S. Park, H.J. Song, D.H. Seo, K.E. Byun, P. Kim, I.K. Yoo, H.J. Chung, K. Kim, Science 336 (2012) 1140–1143.
[30] L. Britnell, R.V. Gorbachev, A.K. Geim, L.A. Ponomarenko, A. Mishchenko, M.T. Greenaway, T.M. Fromhold, K.S. Novoselov, L. Eaves, Nat. Commun. 4 (2013) 1794.
[31] W. Jie, X. Chen, D. Li, L. Xie, Y.Y. Hui, S.P. Lau, X. Cui, J. Hao, Angew. Chem. Int. Ed. Engl. 54 (2015) 1185.
[32] W. Kim, C. Li, F.A. Chaves, D. Jimenez, R.D. Rodriguez, J. Susoma, M.A. Fenner, H. Lipsanen, J. Riikonen, Adv. Mater. 28 (2016) 1845.
[33] X. Li, M.W. Lin, A.A. Puretzky, J.C. Idrobo, C. Ma, M. Chi, M. Yoon, C.M. Rouleau, I.I. Kravchenko, D.B. Geohegan, K. Xiao, Sci. Rep. 4 (2014) 5497.
[34] Y. Huang, E. Sutter, J.T. Sadowski, M. Cotlet, O.L.A. Monti, D.A. Racke, M.R. Neupane, D. Wickramaratne, R.K. Lake, B.A. Parkinson, P. Sutter, ACS Nano 8 (2014) 10743.
[35] X. Zhou, Q. Zhang, L. Gan, H. Li, T. Zhai, Adv. Funct. Mater. 26 (2016) 4405–4413.
[36] X. Yuan, L. Tang, S. Liu, P. Wang, Z. Chen, C. Zhang, Y. Liu, W. Wang, Y. Zhou, C. Liu, N. Gao, J. Zou, P. Zhou, W. Hu, F. Xiu, Nano Lett. 15 (2015) 3571–3577.
[37] Y.B. Yang, J.K. Dash, A.J. Littlejohn, Y. Xiang, J. Shi, L.H. Zhang, K. Kisslinger, T.M. Lu, G.C. Wang, Crys. Growth Des. 16 (2016) 961–973.
[38] L.A. Burton, T.J. Whittles, D. Hesp, W.M. Linhart, J.M. Skelton, B. Hou, R.F. Webster, G. O'Dowd, C. Reece, D. Cherns, D.J. Fermin, T.D. Veal, V.R. Dhanak, A. Walsh, J. Mater. Chem. A 4 (2016) 1312.
[39] X. Zhou, Q. Zhang, L. Gan, H. Li, J. Xiong, T. Zhai, Adv. Sci. 3 (2016) 1600177.
[40] X. Li, M.W. Lin, A.A. Puretzky, J.C. Idrobo, C. Ma, M. Chi, M. Yoon, C.M. Rouleau, D.B. Kravchenko II, K. Xiao Geohegan, Sci. Rep. 4 (2014) 5497.
[41] X. Li, L. Basile, M. Yoon, C. Ma, A.A. Puretzky, J. Lee, J.C. Idrobo, M. Chi, C.M. Rouleau, D.B. Geohegan, K. Xiao, Angew. Chem. Int. Ed. Engl. 54 (2015) 2712.
[42] X. Gong, M. Tong, Y. Xia, W. Cai, J.S. Moon, Y. Cao, G. Yu, C.L. Shieh, B. Nilsson, A.J. Hegger, Science 325 (2009) 1665.
[43] J. Kaniewski, J. Piotrowski, Opto-electron. Rev. 12 (2004) 139.
[44] M.M. Furchi, A. Pospischil, F. Libisch, J. Burgdorfer, T. Mueller, Nano Lett. 14 (2014) 4785–4791.
[45] N.J. Huo, J. Kang, Z.M. Wei, S.S. Li, J.B. Li, S.H. Wei, Adv. Funct. Mater. 24 (2014) 7025–7031.
[46] Y. Deng, Z. Luo, N.J. Conrad, H. Liu, Y. Gong, S. Najmaei, P.M. Ajayan, J. Lou, X. Xu, P.D. Ye, ACS Nano 8 (2014) 8292–8299.
[47] M.S. Choi, D. Qu, D. Lee, X. Liu, K. Watanabe, T. Taniguchi, W.J. Yoo, ACS Nano 8 (2014) 9332–9340.
[48] F. Wang, Z. Wang, K. Xu, F. Wang, Q. Wang, Y. Huang, L. Yin, J. He, Nano Lett. 15 (2015) 7558–7566.
[49] R. Saran, R.J. Curry, Nat. Photonics 10 (2016) 81.
[50] P. Perumal, R.K. Ulaganathan, R. Sankar, Y.M. Liao, T.M. Sun, M.W. Chu, F.C. Chou, Y.T. Chen, M.H. Shih, Y.F. Chen, Adv. Funct. Mater. 26 (2016) 3630.
[51] D.B. Velusamy, R.H. Kim, S. Cha, J. Huh, R. Khazaeinezhad, S.H. Kassani, G. Song, S.M. Cho, S.H. Cho, I. Hwang, J. Lee, K. Oh, H. Choi, C. Park, Nat. Commun. 6 (2015) 8063.
[52] S.R. Tamalampudi, Y.Y. Lu, U.R. Kumar, R. Sankar, C.D. Liao, B.K. Moorthy, C.H. Cheng, F.C. Chou, Y.T. Chen, Nano Lett. 14 (2014) 2800.
[53] H. Cai, J. Kang, H. Sahin, B. Chen, A. Suslu, K. Wu, F. Peeters, X. Meng, S. Tongay, Nanotechnology 27 (2016) 065203.
[54] R. Lu, J. Liu, H. Luo, V. Chikan, J.Z. Wu, Sci. Rep. 6 (2016) 19161.
[55] D.J. Late, B. Liu, J. Luo, A. Yan, H.S.S.R. Matte, M. Grayson, C.N.R. Rao, V.P. David, Adv. Mater. 24 (2012) 3549–3554.
[56] S. Kim, A. Konar, W.S. Hwang, J.H. Lee, J. Lee, J. Yang, C. Jung, H. Kim, J.B. Yoo, J.Y. Choi, Y.W. Jin, S.Y. Lee, D. Jena, W. Choi, K. Kim, Nat. Commun. 3 (2012) 1011.